Miewon Jung

Thesis for the Degree of Master

Study on Hydrogen Permeation of Ce-based Ceramics Membrane

2014

Graduate School of Sungshin University

Department of Chemistry

Jihye Park

Study on Hydrogen Permeation of Ce-based Ceramics Membrane

Miewon Jung

Submitting a master's thesis of
Chemistry

Date (November, 2013)

Graduate School of Sungshin University

Department of Chemistry

Jihye Park

Approval

Confirming the master's thesis written

by Jihye Park.

Examiner _____ Seal

Examiner _____ Seal

Examiner _____ Seal

Graduate School of Sungshin University

ABSTRACT

The objective of this work is to enhance the hydrogen permeation as well as selectivity between H_2/CO gases at various temperatures.

Porous SiC ceramics were prepared by using recycled SiC sludge, which is an industrial waste generated from solar cell industry. In order to enhance the hydrogen permeation, Cerium oxide (CeO_2) was synthesized by sol-gel process and SiC-CeO_2 composite membrane via dip-coating method was fabricated to evaluate of hydrogen permeation.

In case of SiC-$CeNiO_3$ membrane, the prepared SiC-$CeNiO_3$ powders mixed with alloying method using a nickel metal powders having a ductility and high mechanical strength was fabricated as Cermet (Ceramic / Metal) composite separation membrane by hot-press-sintering (HPS). We have discussed the effects of the hydrogen separation membrane, which is produced in Cermet system. However, there is a drawback in contrast with the

selectivity in spite of that the permeation was increased. In addition, Ce-based membrane was on reaction of reduction under the hydrogen atmosphere.

For this reason, Lanthanum ($La_2Ce_2O_7$) complex oxides were synthesized, membrane permeability and selectivity of values on the experimental were obtained improved results. The prepared powders and composite membranes were investigated by XRD, FE-SEM, BET techniques. By using the hydrogen permeation membrane, the evaluation under a variety of pressures and temperatures was carried out through H_2 and CO gas.

CONTENTS

LIST OF FIGURES

Chapter 1.

Chapter 2.

Chapter 3.

Chapter 4.

Chapter 1

“Hydrogen Permeation of the $La_2Ce_2O_7$ Composite Membrane”

1.1 Introduction

As the traditional energy materials, such as coal, oil and gas become further depleted, hydrogen which is well-known for clean energy carrier has received attention to be the most promising alternative resource [1-2]. Recently, hydrogen energy have various ways of being developed, especially, membrane-based separation process are the primary concern used on the polymeric, metallic, mixed matrix and ceramic membranes has a lot of advantages: cost effective, high recovery factor and production of high-purity hydrogen [3-4]. In accordance with the type of materials, hydrogen separation membranes can be classified such as the categories: polymeric membranes, porous membranes, dense metal membranes and proton conducting membranes. Above all, proton conducting membrane which may be classified into the following groups: dense ceramic membranes and composite

ceramic metal (cermet) membranes have various properties in terms of the hydrogen permeation membrane. Dense ceramic membranes are included on structure by perovskite and non-perovskite membrane as well. The non-perovskite structured membrane for hydrogen separation is well-known the fluorite structure [5]. In previous work, we have studied ceramic membrane which was composed by CeO_2 because ceria-based materials are one of the most leading ionic conductors for intermediate-temperature SOFC and sensor application [6-7]. In order to improve the stability of Ce-based membrane, different approaches have been applied as the synthesis of CeO_2 with La_2O_3 material. The derived via sol-gel process Lanthanum cerate ($La_2Ce_2O_7$) membrane with a permeation for H_2 separation is chemically and mechanically stable. Among the type of oxides, the fluorite structured $La_2Ce_2O_7$ have been on the spotlight as an electrode component in proton conducting fuel cells and non-perovskite structure as already mentioned [8-9]. The $A_2B_2O_7$ oxide has shown potential performance as fast ionic conductors. In addition, the complex oxide is well-known for applications

such as hydrogen sensors and fuel cells because of its considerable proton conduction at high temperature [10]. The fluorite structure indicates good chemical stability compared to proton conductor called perovskite structure. Furthermore, the $La_2Ce_2O_7$ composite oxide was used to thermal barrier coating (TBCs) [11-12].

In this paper, we will discuss the recent work regarding the fabrication of the $La_2Ce_2O_7$ via sol-gel process for hydrogen permeation. The main purpose of this study is to enhance properties of perm-selectivity and permeation as hydrogen separation membrane.

1.2 Experimental

1.2.1 Preparation of the $La_2Ce_2O_7$ powders

Lanthanum (III) nitrate hexahydrate ($La(NO_3)_3 \cdot 6H_2O$) (CAS No. 10277-73-7, Aldrich) and Cerium (III) nitrate hexahydrate ($Ce(NO_3)_3 \cdot 6H_2O$) (CAS No.10294-41-4, Aldrich) with a purity of 99% were dissolved in distilled water with a molar ratio of $La(NO_3)_3 \cdot 6H_2O$: $Ce(NO_3)_3 \cdot 6H_2O$ =1:1 at 353 K. And then, nitric acid (HNO_3) as an acid catalyst was added and the concentration of pH was adjusted. The sol solution was refluxed for overnight and the gel powders obtained by drying at 393 K for 24 h were sintered to complete sol-gel synthesis at 1473 K under air condition.

1.2.2 Fabrication of the $La_2Ce_2O_7$ membranes

For the fabrication of the membranes based on $La_2Ce_2O_7$ and CeO_2 powders respectively, 10 wt% of polyvinyl alcohol (PVA)

used as a binder was prepared for hydrogen permeation. The each powder were pressed by uniaxial pressing at 100 bar with a diameter of 14.5 mm and a thickness of 2 mm and sintered at 1173 K under Ar condition.

1.2.3 Characterization

The phase composition of crystal structure was determined by X-ray diffraction (Bruker D8, Focus, Cukα, 40Kv, 40mA). Microstructure of the powders and membranes was observed using Field Emission-Scanning Electron Microscope (JEOL-JMS 7500F). Pore size distribution was analyzed by Barrett-Joyner-Halenda method and the Brunner-Emmett-Teller (BELSORP-max, mini II) method was measured by the adsorption-desorption of N_2 gas for surface area (m^2/g). Hydrogen permeation measurement was performed at elevated temperatures and the devices which are consisted of a pressure controller, mass flow controller (MFC) and stainless steel 1.4-inch cell equipment was constructed as to withstand on high temperature.

1.3 Results and Discussion

The $La_2Ce_2O_7$ powders after the sintering at 773 K are observed to be crystalline, as defined from XRD patterns presented in Fig. 1. The results of the XRD analysis on the $La_2Ce_2O_7$ powders were shown that corresponds to a cubic fluorite structure and space group Fm3m. No other peaks attributable to individual oxides were detected. The XRD pattern of the $La_2Ce_2O_7$ was similar to the CeO_2 with a small shift of the lattice parameter. Furthermore, while the sintering temperature of the $La_2Ce_2O_7$ powders was elevated from room temperature to 1473 K, the powders were unaffected, which means that the $La_2Ce_2O_7$ powders have high phase stability. In case of the CeO_2 powders, the diffraction peaks is indexed of a cubic structure (a=b=c=5.40370 nm).

FE-SEM images of the La_2O_3, CeO_2 and $La_2Ce_2O_7$ powders prepared after sintering at 1173 K are reported in Fig. 2. The La_2O_3 powders show the occurrence of large clusters by crystallites aggregation, whereas CeO_2 and $La_2Ce_2O_7$ powders shown less rough surface without clustering. In agreement with

the results of structures on XRD, the CeO_2 and the $La_2Ce_2O_7$ powders have similar morphology.

As demonstrated in Fig. 3, the $La_2Ce_2O_7$ membrane was tested for separation membrane by H_2 and CO gases at elevated temperatures. In Fig. 3, the hydrogen permeation fluxes of the both membranes on the $La_2Ce_2O_7$ and the CeO_2 membrane are shown the decreasing tendency with increasing temperature. A study on general ceramic materials announced following the surface diffusion and Knudsen diffusion, which as the decreasing of hydrogen permeation flux, as increasing temperature. The fluxes of H_2 and CO gases permeation were reduced with a temperature over 298 K. For the permeation of hydrogen gas, the flux is proportional to the pressure, whereas it is proportional to the temperature. According to the results of BET adsorption and desorption (Fig. 5), the membranes are compiled by type IV hysteresis loop isotherms, which is indicating that the mesoporous.

At the previous work, contrary to $La_2Ce_2O_7$ composite membrane, the CeO_2 membrane was reaction on reduction.

However, as can be seen in Fig. 6, the images of $La_2Ce_2O_7$ composite membrane after permeation tests by H_2 and CO gases are shown, where no change is discovered on the $La_2Ce_2O_7$ composite membrane. Besides, the $La_2Ce_2O_7$ composite membrane is stable in terms of hydrogen permeation test. Hydrogen permeation flux of the $La_2Ce_2O_7$ membrane, which has the highest value, was obtained at 7.27×10^{-5} mol/m^2sPa, 303 K. The reaction enthalpy (ΔH°) was calculated as - 4.30 kJ/mol by Arrhenius's plot.

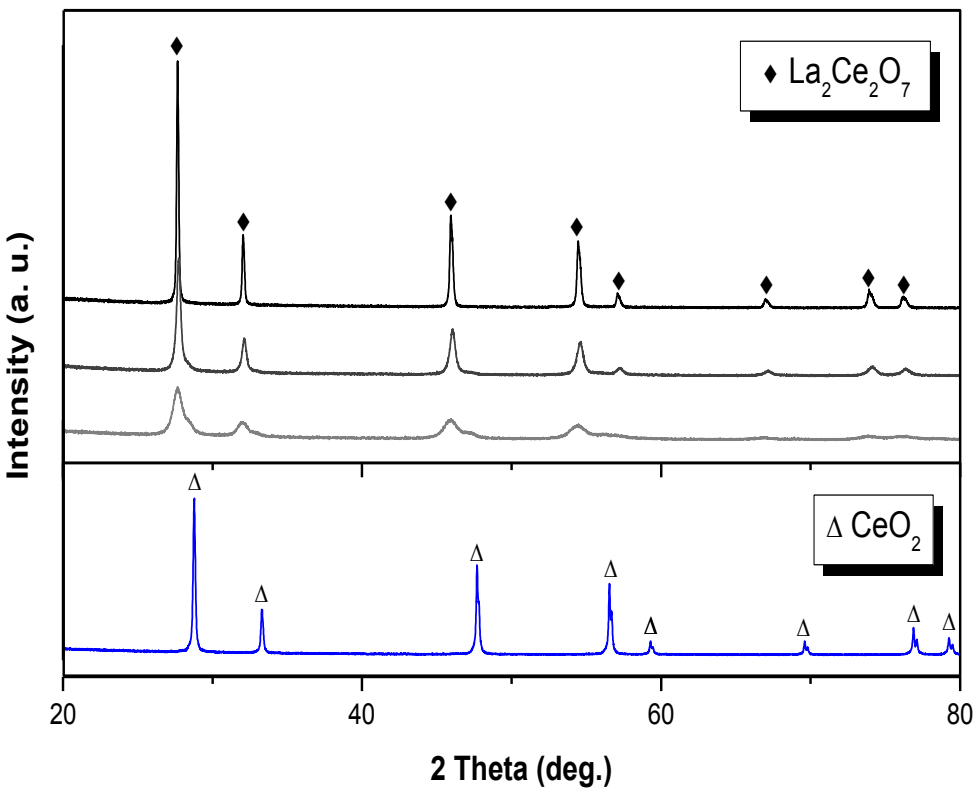

Fig. 1. XRD patterns of powders

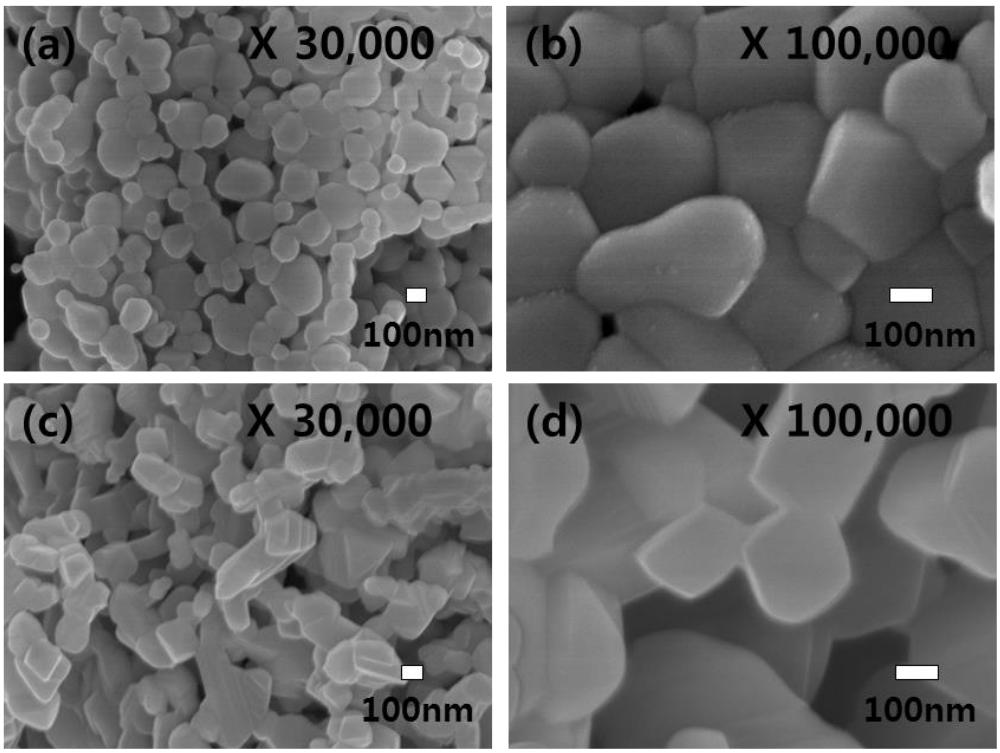

Fig. 2. FE-SEM images of (a, b) of CeO_2 and (c, d) of $La_2Ce_2O_7$ powders.

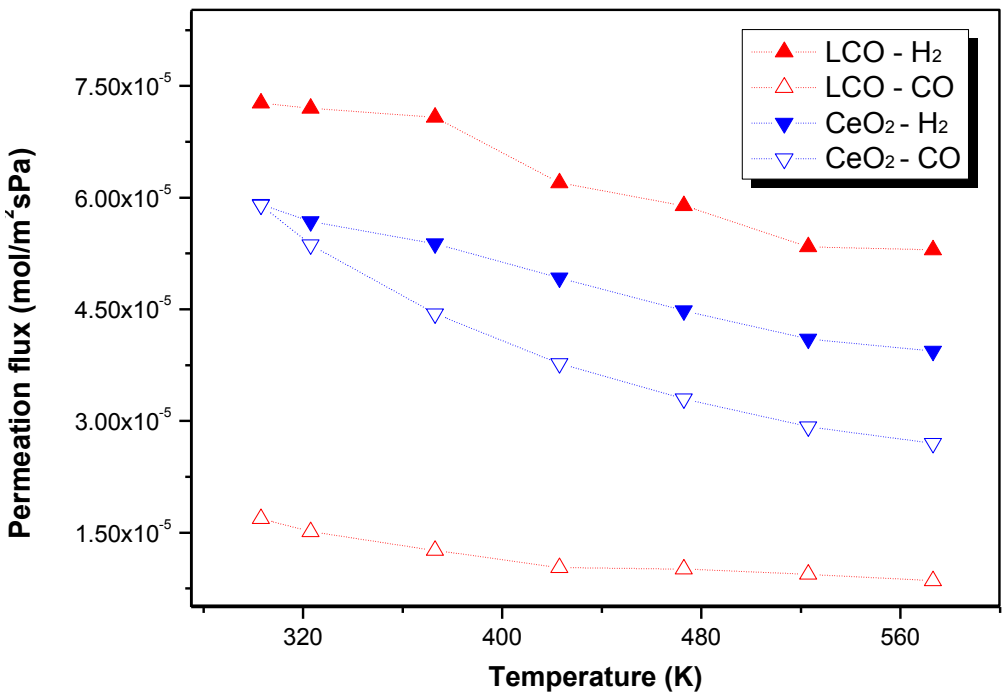

Fig. 3. Permeation fluxes (mol/m^{2}sPa) of $La_2Ce_2O_7$ (LC) and CeO_2 (C) membranes at elevated temperatures (RT-573 K) between H_2 and CO gases.

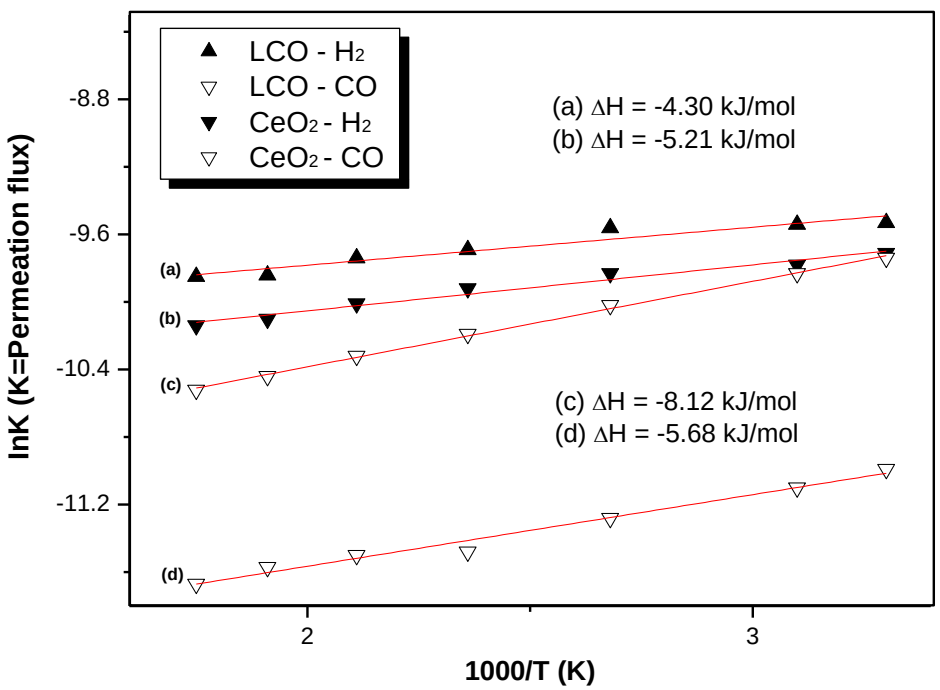

Fig. 4. Arrhenius plots of permeation flux on the $La_2Ce_2O_7$ (LC) and CeO_2 (C) membranes.

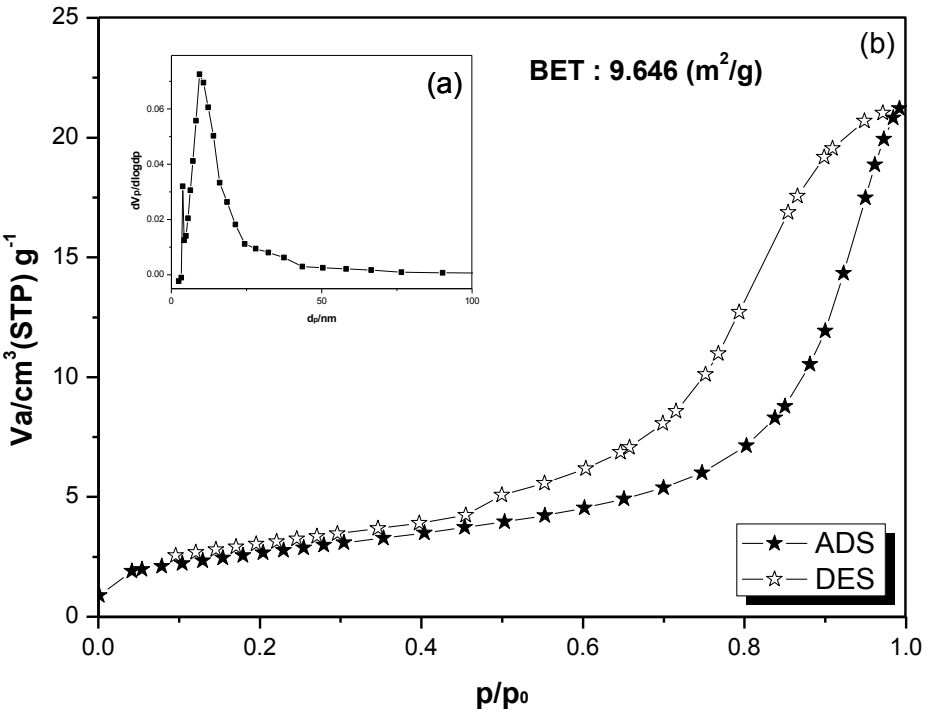

Fig. 5. (a) Pore size distribution and (b) N_2 adsorption-desorption isotherms of the $La_2Ce_2O_7$ composite membrane.

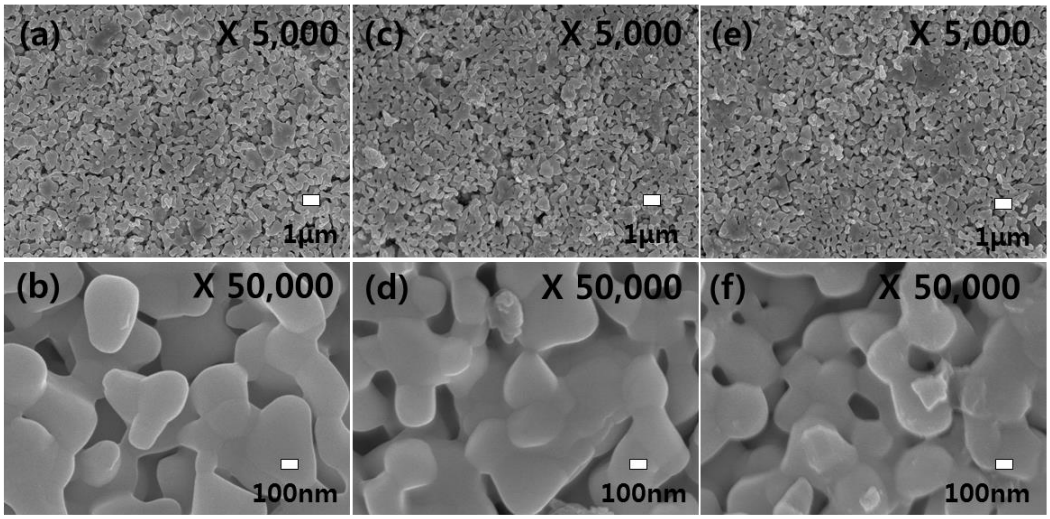

Fig. 6. FE-SEM images of (a, b) before, (c, d) after hydrogen permeation test and (e, f) CO permeation test for the $La_2Ce_2O_7$ composite membrane.

1.4 Conclusion

Sol-gel derived the $La_2Ce_2O_7$ powders with nano-crystalline structure have been successfully prepared. The $La_2Ce_2O_7$ powders using polyvinyl alcohol (PVA) as a binder were fabricated and investigated to evaluate the hydrogen permeation. As the increase of the temperature, the $La_2Ce_2O_7$ composite membrane responds as the Knudsen and surface diffusion that observed by permeation test on the membrane. The fluxes of permeation have been decreased as increasing temperature. Selectivity on permeation via H_2/CO gases is the highest when the temperature is reached at 573 K. Compared with the CeO_2 membrane, there is higher selectivity that flux in $La_2Ce_2O_7$ membrane shows significant increase selectivity because of the chemically stable under the hydrogen permeation.

Chapter 2

"Dip-coating of Nano-sized CeO_2 on SiC Membrane and Its Effect on Thermal Diffusivity[1]"

2.1 Introduction

Porous SiC ceramic is one of the most promising materials used as catalyst carrier, heat-exchanger and diverse filter due to their thermo-chemical and mechanical stability [1-2]. The porosity of SiC membrane can be affected by the metal oxide additives [3]. Especially, cerium oxide adding on SiC membrane could influence on the porosity and pore size which is related with their thermal behavior [2-4]. To fabricate SiC ceramic based membrane, the sol-gel method is the good choice to make metal oxide powder or precursor sol solution with good stoichiometric control. From beginning step of the chemical synthesis, it is possible to control on the ratio of the composition and to have homogeneous sol solution with uniform distribution even at low synthetic

[1] Journal of Nanoscience and Nanotechnology (In Press)

temperature [5]. For making the homogeneous and crack-free monolayered CeO_2-SiC dip-coated membrane, different coating times were applied for this study. It was compared between traditional mixing and dip-coating process in terms of porosity, microstructure analysis and densification of the membrane. Thermal diffusivity measurements with relate to porosity will be discussed on these SiC membranes with changing temperatures.

2.2 Experimental

2.2.1 Preparation of the cerium oxide

$Ce(NO_3)_3 \cdot 6H_2O$ (99%, Aldrich) was dissolved into distilled water and 0.16 mol of the nitric acid was added as a catalyst (pH=1.5). This sol solution was used at proper viscosity or it was further stirred with refluxing for 24h. Then, it was dried and heat-treated to obtain the cerium oxide powder at 900 °C.

2.2.2 Fabrication of CeO_2-SiC membranes

The purified SiC ceramic (325 mesh) was ball-milled with hydridopolycarbosilane in cyclohexane for 24h. The homogenized powder was dried at 150 ℃ for 1h. The purified SiC ceramic alone or cerium oxide with SiC ceramic (2 : 98 wt.%) were pressed by uniaxial pressing at 200 bar. These two kinds of membranes were pressureless sintered at 900 ℃ under Ar atmosphere. The heat-treated SiC membrane was dip-coated by the cerium oxide

precursor sol solution with controlling viscosity (1.60 ~ 1.70 cP). The dip-coating process was performed 12 or 60 times at a constant dipping speed of 0.1 mm^2/s. These membranes were heat treated with air at 900 ℃.

2.2.3 Characterization

The Rietveld refinement of XRD (Bruker D8 Focus, Cukα, 40kV, 40mA) on the purified SiC ceramic were 97.81 % of α-SiC (hexagonal), 1.33 % of C and 0.86 % of Si (cubic). To observe the surface and cross section, FE-SEM (JEOL-JMS 7500F) with magnification of 1,000 and 100,000 were utilized. The BET surface area (BELSORP-max, mini II) was analyzed by the adsorption of N_2 gas. In order to measure the porosity and density, Archimedes method was used. Thermal diffusivity was measured by Laser flash method (NETZSCH LFA 447).

2.3 Results and Discussion

SiC peaks were observed more outstanding α-phase of hexagonal form than β-phase of cubic form in all cases in Fig. 1. The cerium oxide peaks having small intensity by dip-coating process were existed with cubic structure (JCPDS file No.03-065-2975, a=5.41100 nm), while these peaks were not shown in the mixing membrane. When this dip-coating process was performed by 60 times, the cerium oxide peaks in (c) were sharper and clearer than those in (b). It is indicated that the phase of cerium oxide is developed by the increase of coating process.

The surface and cross sectional images of the CeO_2-SiC composite membranes have smooth surface and homogeneous with crack-free features in Fig. 2. The spherical particle shape was observed from the well resolved surface diagram and it was attributed to cerium oxide formation on the SiC surface. The cross sectional images look similar at low-magnification with 1,000 in Fig. 2 (d) and (e). But enlarged images with 100,000 appear distinct difference. The uniform and dense dip-coating of the

CeO_2 on the surrounding of the SiC particles in membrane could obtain by dip-coating 60 times. According to IUPAC, all isotherms show a typical IV model and a HI hysteresis loop that is representative of mesopore with the uniform pore size distribution in Fig. 3 (a). A type N_2 hysteresis is associated with cylinder pores or voids. Average pore size was around 4~6 nm and mesoporous with uniform distribution in all cases. The membrane by mixing process has the highest pore volume and its value was the lowest when dip-coating process was applied by 60 times. Pore volume in the mesoporous SiC matrix had a decreasing trend as the densification of the membrane by increased dip-coating times proceeded in Fig. 3 (b).

Thermal diffusivity could only measure for the membranes by mixing and also dip-coating by 12 times. Fig. 4 shows a decreasing tendency with increasing temperatures. This value for dip-coating was less than those of mixing one at all of the temperatures. The dip-coated membrane had the highest value as 2.39×10^{-4} mm^2/s at RT. Porosity and density by Archimedes method on mixing sample were 27.43 % and 3.17 g/cm^3,

respectively (Table 1). Porosity was reduced to 22.87 % by dip-coating process and this reduced porosity could influence on the thermal diffusivity [4].

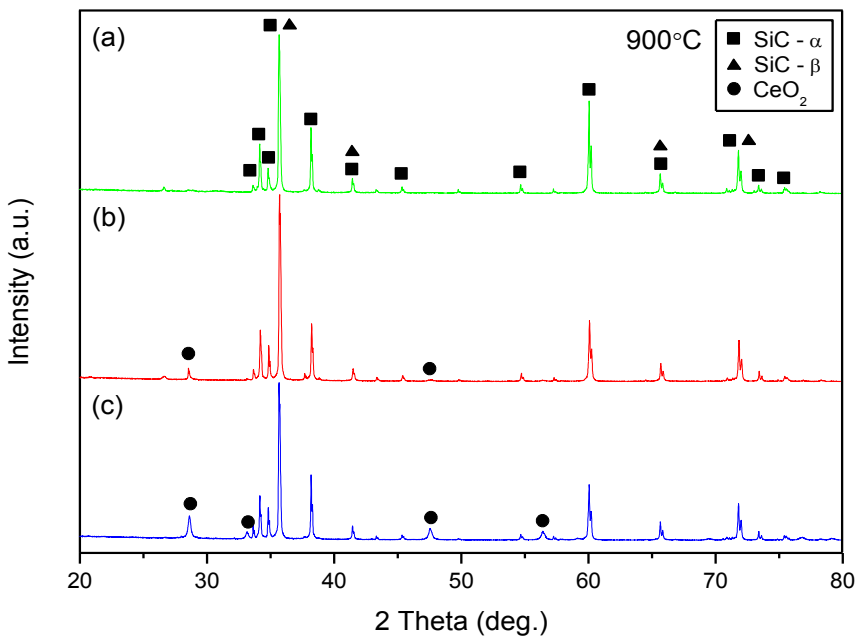

Fig. 1. XRD patterns of CeO_2-SiC composite membranes prepared by (a) mixing, (b) dip-coating 12 times and (c) dip-coating 60 times.

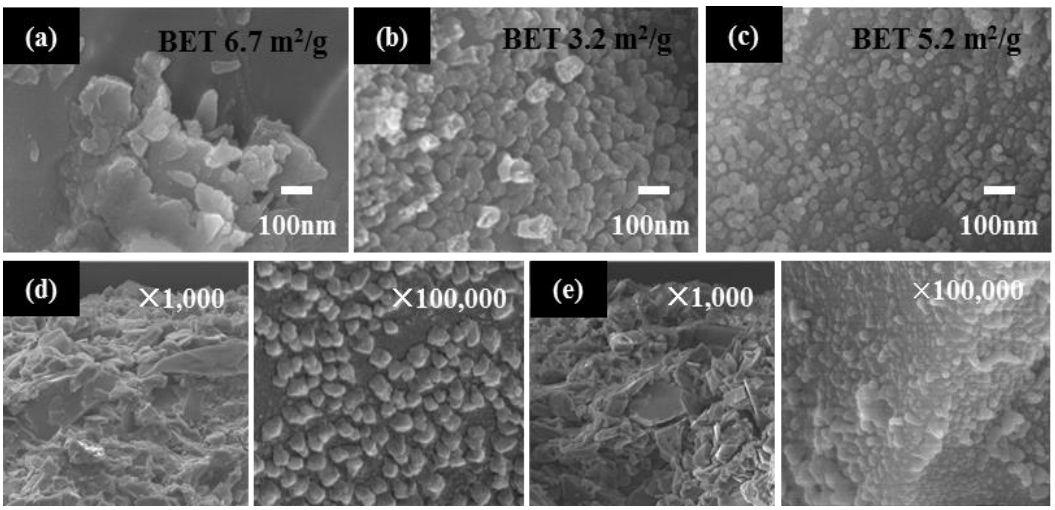

Fig. 2. The surface photographs of (a) mixing, (b) 12 times and (c) 60 times by dip-coating with 100,000. Cross sectional images of (d) 12 times and (e) 60 times by dip-coating with 1,000 are enlarged by 100,000 in the right side of the (d) and (e).

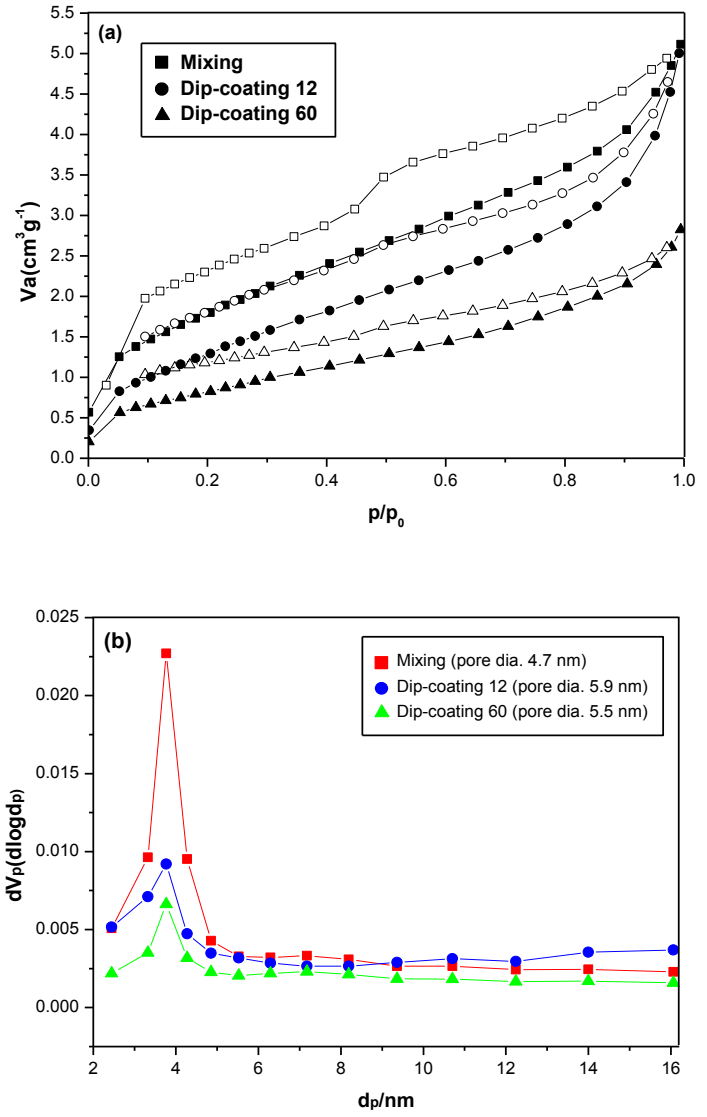

Fig. 3. (a) N_2 adsorption-desorption isotherms and (b) the distribution of pore diameters by BJH method.

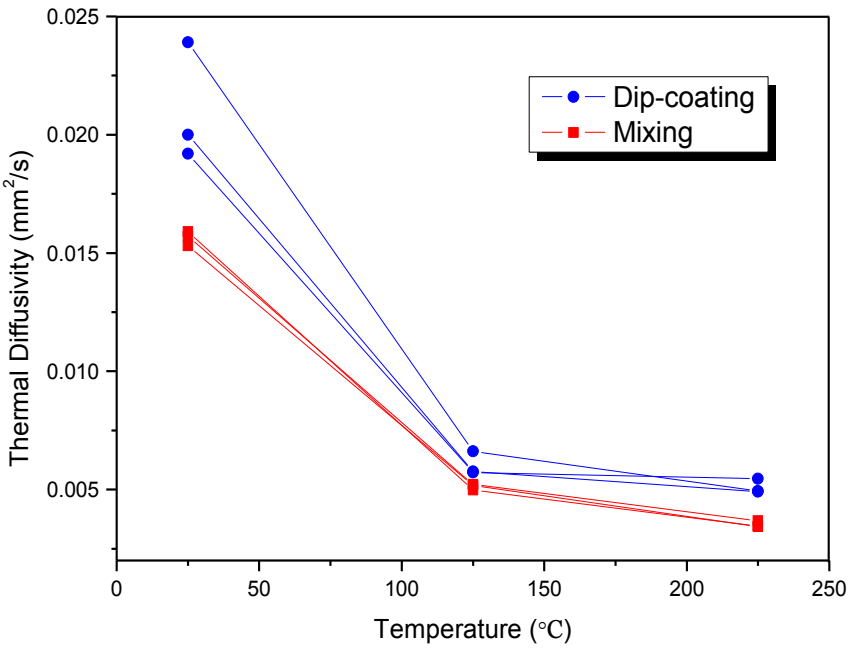

Fig. 4. Measured thermal diffusivity of CeO_2–SiC membranes.

2.4 Conclusion

Nano-sized cerium oxide particles on the surface of the SiC membrane were successfully fabricated by dip-coating. With repeating the number of times of the dip-coating, the membrane was densified. The benefit of dip-coating is not only affected the porosity and density, but also promoted the formation of nano-sized cerium oxide on the surface and cross section of the membrane. Dip-coating process could control on the porosity and density of the membrane and this affects the thermal diffusivity.

Chapter 3

"Hydrogen Permeation of SiC-CeO_2 Composite Membrane by Dip-coating Process[2]"

3.1 Introduction

Hydrogen energy is of considerable interest for various applications such as polymer electrolyte membrane fuel cells (PEMFCs) and supply and storage carriers, and a great deal of research accordingly has been conducted on separation, production, and transportation of hydrogen [1-2].

Also, silicon carbide (SiC) is an attractive candidate for hydrogen separation ceramic membranes because of its good thermal properties and hardness at high temperature. In addition, the SiC is a promising material for use in catalyst carriers and filters owing to its excellent thermal, mechanical and chemical stability [3-4].

---

[2] Journal of the Korean Ceramic Society (Vol. 50, No. 6, pp. 485-488, 2013)

Especially, recycled SiC sludge from the solar cell industry can be used because it is ecofriendly and this would concurrently reduce the amount of industrial waste [5-6]. A number of oxides have been added to SiC matrices to prepare dense membranes and control the microstructure, including the pore size in particular. The use of CeO_2 leads to improved proton conductivity and it is appropriate for a hydrogen separation membrane because it induces electron conductivity by reduction [7-8]. In order to prepare the CeO_2 dip-coated SiC based membrane, a sol-gel process was used to cover the SiC membrane as a first layer. The sol-gel process is known to afford good control of stoichiometry.

Moreover, it is an effective method to control the pore size and distribution for obtaining high-surface area supports [9]. In this study, we discuss the fabrication of a SiC-CeO_2 membrane by a dip-coating process and the mechanism underlying the difference in H_2 and CO gases flux between SiC and SiC-CeO_2 membrane.

3.2 Experimental

3.2.1 Preparation of the CeO_2 sol solution

Cerium (III) nitrate hexahydrate ($Ce(NO_3)_3 \cdot 6H_2O$) (99%, CAS No.10294-41-4, Aldrich) was dissolved in distilled water with a mole ratio of Ce : H_2O = 1 : 100 at 353 K. As an acid catalyst, nitric acid (HNO_3) was added and refluxed for overnight to obtain the CeO_2 sol solution via sol-gel process.

3.2.2 Fabrication of the SiC-CeO_2 membrane by dip-coating process

SiC (325 mesh) (BIT. Co., Ltd) generated from solar cell industry was used for a support membrane. Purified SiC powders were ball-milled with ally-hydridopolycarbosilane (AHP CS) for 24 h. The well-blended SiC powders were pressed in a mold with a diameter of 14.5 mm and a thickness of 2 mm by uniaxial pressing at 20 MPa. The molded membrane was pressurelessly

sintered at 1173 K for 2 h under Ar atmosphere. For the dip-coating process, the CeO_2 sol solution was prepared at 1.60 cP viscosity. The fabricated SiC membrane designed for use as a support was dip-coated by CeO_2 sol solution at a constant dipping speed of 0.1 mm^2/s 60 times. This membrane was heat-treated to complete the formation of a dense CeO_2 layer on the SiC membrane at 1173 K for 2 h under an air atmosphere.

3.2.3 Characterization and Gas permeation test

The phase composition of the crystal structure on the SiC-CeO_2 membrane was determined by X-ray diffraction (Bruker D8, Focus, Cukα, 40 Kv, 40 mA) (λ = 1.5406) followed by Rietveld structure refinement for a quantitative analysis. The surface microstructure and morphology of the membrane were observed using a Field Emission-Scanning Electron Microscope (JEOL-JMS 7500F). The pore size distribution was analyzed by the Barrett-Joyner-Halenda (BJH) method. The Brunner-Emmett-Teller (BET) (BELSORP-max, mini II) technique was used to measure the

adsorption-desorption of N_2 gas according to surface area (m^2/g). A permeation measurement analyzer (Fig. 1), which consisted of a pressure controller, mass flow controller (MFC) and stainless steel 1.4-inch cell was constructed to withstand high temperature. The permeation performance of H_2/CO gases was evaluated at room temperature to 573 K under 0.03 MPa.

3.3 Results and Discussion

From the XRD spectrums, the SiC membrane dip-coated by CeO_2 and the untreated SiC membrane are observed to be crystalline, as presented in Fig. 2. Based on the results of the crystalline phase analysis, SiC peaks were assigned to α-phase of a hexagonal and β-phase of a cubic structure in all cases. After the dip-coating process, CeO_2 peaks having small intensity indicated that CeO_2 existed as nanoparticles and the diffraction peaks are indexed to a cubic structure (JCPDS file No.03-065-2975). By means of Rietveld refinement, it was observed that the crystal size of CeO_2 was reduced from an initial value of 42.5 nm to 38.4 nm after the test.

FE-SEM images of the membranes prepared after sintering at 1173 K are provided in Fig. 3. The membranes appear to be similar at low magnification, but enlarged images (×10,000) in Fig. 3(d) show obvious differences with the presence of large grains by crystallite aggregation. In agreement with the results of XRD spectrums, the morphology of the layered CeO_2 coating is

characterized by a particle size reduction, as shown in Fig. 4. The CeO_2 particles contracted due to a strong tendency toward reduction. The particle size of CeO_2 is 35 ~ 50 nm in the FE-SEM data, consistent with the results of XRD Rietveld refinement.

Porosity, determined by the Archimedes method, of the SiC membrane and SiC-CeO_2 membrane was 27.43% and 21.87%, respectively. The porosity of the SiC-CeO_2 membrane was reduced by the dip-coating process. The total pore volume and pore size of the SiC-CeO_2 membrane are shown in Fig. 5. According to the results of a N_2 adsorption-desorption analysis, the SiC-CeO_2 membrane exhibits a typical type IV isotherm, with a H_2 hysteresis loop defined by IUPAC (International Union of Pure and Applied Chemistry). This indicates a mesoporous structure with the follow ing distinct properties. The membrane developed a H_2 hysteresis loop, demonstrating the existence of ink-bottlelike pores, each having a narrow entrance and a large cavity, as shown in Fig. 5(a). The corresponding BJH pore size distributions for this membrane are narrow with average pore diameter of 5.9 nm, as indicated in Fig. 5(b).

Fig. 6 summarizes the results of the permeation flux (mol/m^2sPa) on the SiC-CeO_2 membrane to assess its performance as a separation membrane with H_2 and CO gases with increasing temperature. The hydrogen permeation flux of the SiC-CeO_2 membrane shows a decreasing tendency with increasing temperature. The hydrogen permeation flux of the SiC-CeO_2 membrane, which was obtained as 8.6×10^{-6} mol/m^2sPa, is the highest at room temperature. Otherwise, the CO permeation flux at the same temperature was obtained as 2.64×10^{-6} mol/m^2sPa.

The permselectivity of H_2/CO is 3.27 $\pm$ 0.015 (standard deviation). On the other hand, the SiC membrane without the dip-coating process shows similar permeation flux between H_2 and CO. The SiC-CeO_2 membrane follows a typical Knudsen diffusion mechanism, where permeation is in inverse proportion to increasing temperature. Fig. 7 shows the Arrhenius plots of all the permeation tests. The SiC-CeO_2 membrane has been reacted as endothermic process within the range of temperature 298 K to 573 K.

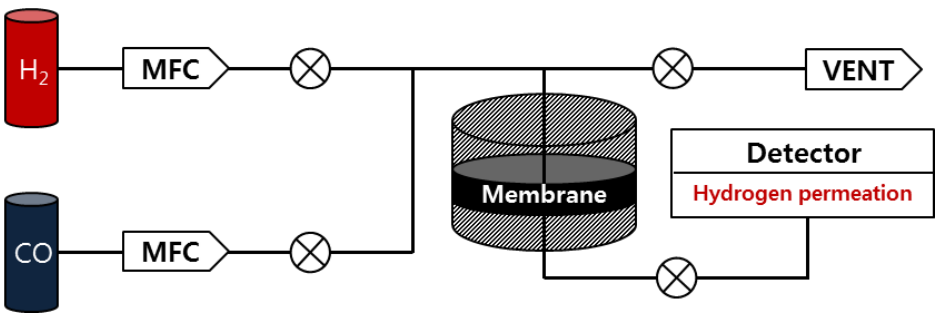

Fig. 1. Schematic of the experimental equipment.

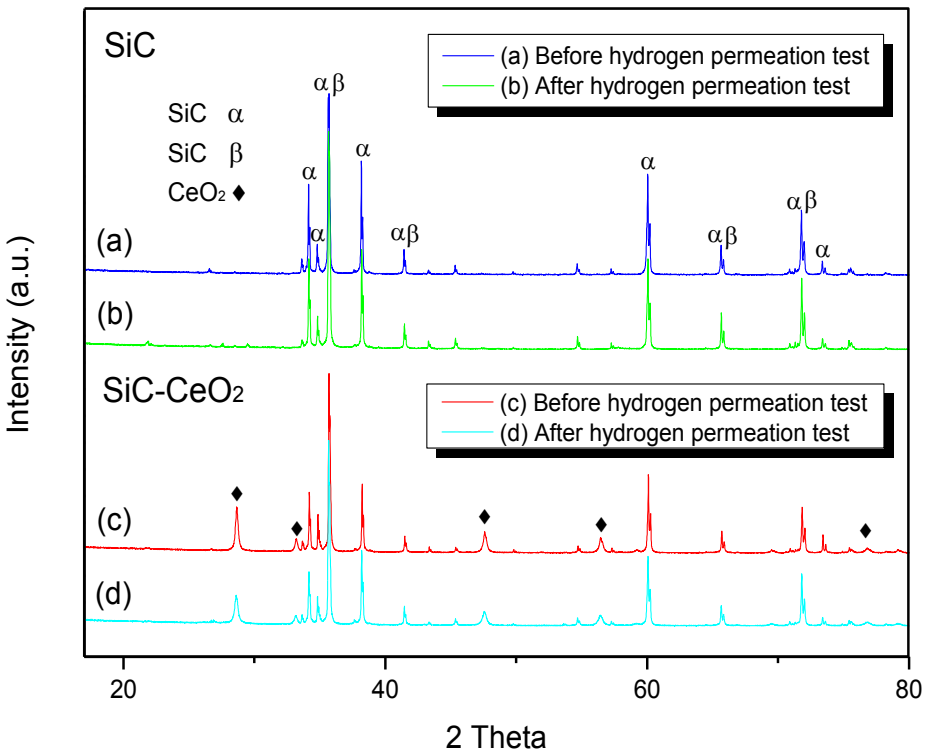

Fig. 2. XRD patterns of the SiC and the SiC-CeO_2 membrane before and after hydrogen permeation tests.

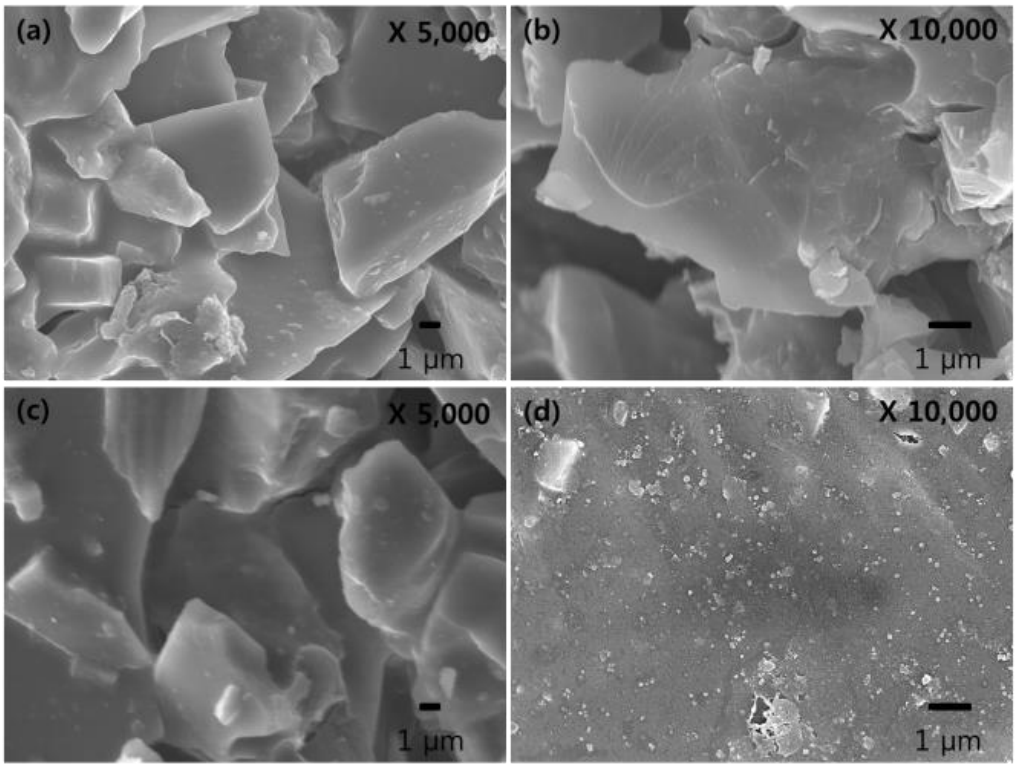

Fig. 3. FE-SEM micrographs of surface with different magnification of (a), (b) on the SiC membrane and (c), (d) on the SiC-CeO_2 membrane.

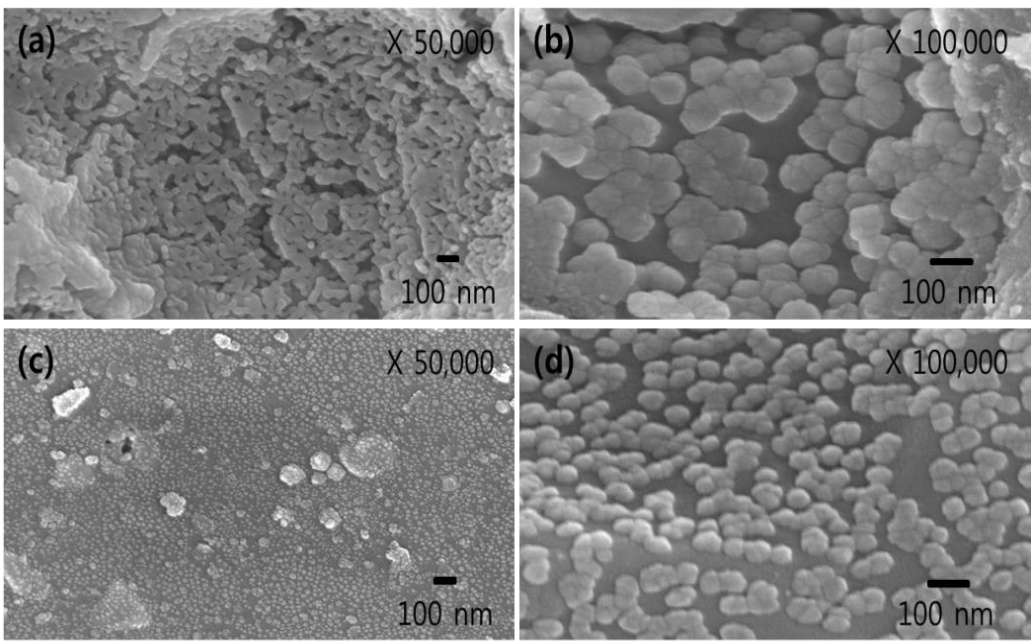

Fig. 4. FE-SEM micrographs of (a) surface, (b) cross section before hydrogen permeation test and (c) surface, (d) cross section after hydrogen permeation test on the SiC-CeO_2 membrane.

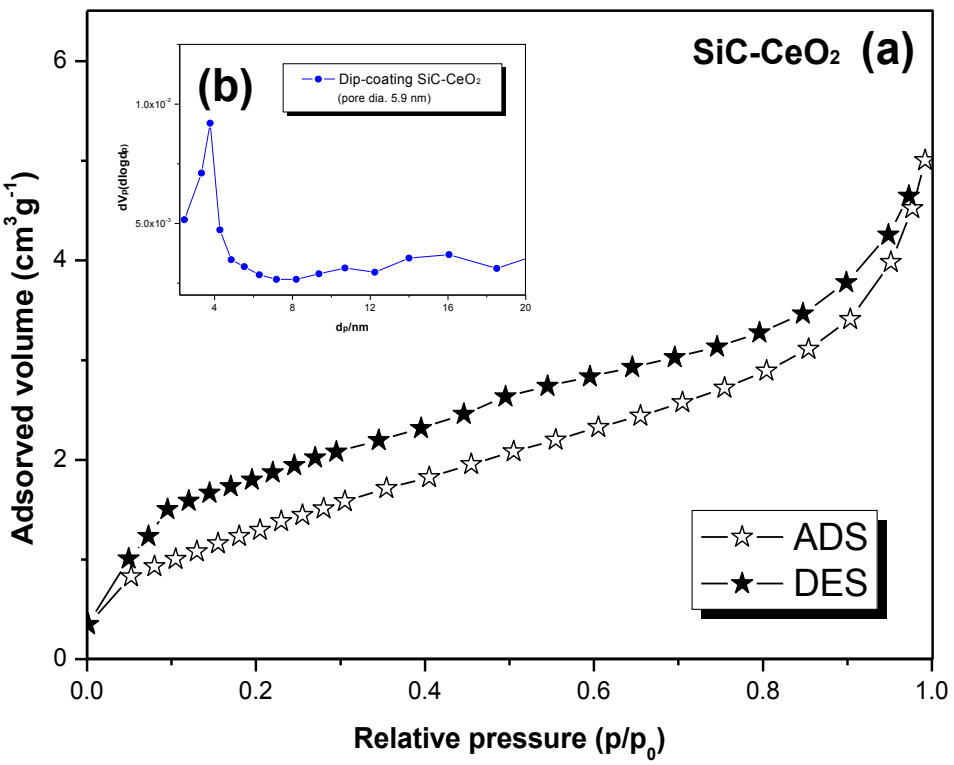

Fig. 5. (a) N_2 adsorption-desorption isotherms and (b) BJH pore size distribution on the $SiC-CeO_2$ membrane.

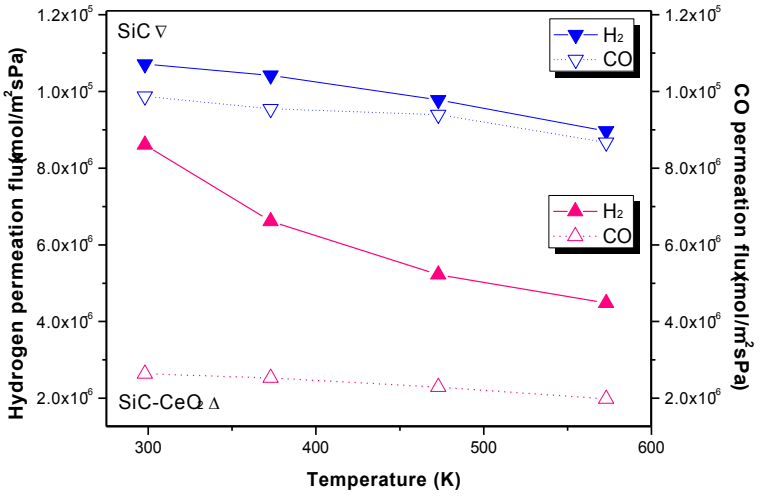

(a)

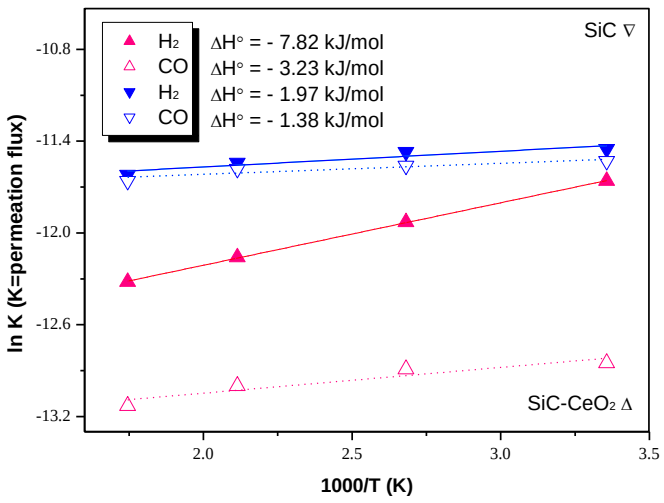

(b)

Fig. 6. (a) Permeation flux of the SiC-CeO_2 membrane at elevated temperatures and (b) Arrhenius plots of permeation flux on the SiC membrane dip-coated by CeO_2.

3.4. Conclusion

Nano-crystalline cerium oxide (CeO_2) particles on the surface of a SiC membrane have been successfully prepared by a dip-coating process. The SiC-CeO_2 membrane was fabricated using a pressureless method and evaluated via gas permeation tests. The dip-coating process not only provided a porous microstructure, but also promoted the formation of nano-sized CeO_2 on the surface and the cross section of the membrane. The dip-coating process could be used to control the porosity and density of the membrane and thereby influence the membrane's gas permeation properties.

Chapter 4

"Fabrication and Characterization of CeO_2-NiO/SiC Membranes for Hydrogen Permeation[3]"

4.1 Introduction

As the resource depletion with the growth in environment issues has been predicted, the demand of hydrogen energy is much more increasing in various categories. Thereby, hydrogen energy, which is able to obtain as a way by storage, separation, production and transportation, is one of the leading candidates for alternative and eco-friendly energy. Especially, the method of hydrogen separation membrane for hydrogen production has been developed with Pd, Pd-alloy and amorphous materials [1-2]. However, within these kinds of materials for the separation membrane occur an irreversible damage caused by bulk sulfide formation and the most negative element of these materials is its high cost [3-5]. For that reason, silicon carbide (SiC) as a support has attracted

[3] Defect and Diffusion Forum (In Press)

notice as ceramic membrane and has been studied in the field of hydrogen separation membranes. Moreover, SiC has the properties of its high thermal conductivity, resistance, corrosion and low thermal expansion coefficient on high temperature, so it is suitable for high temperature hydrogen separation [6-7]. Recently, Lian and co-workers [8] have reported that ceramics based on cerium oxides (CeO_2) have been studied because of their good ion conductivity in solid oxide fuel cell (SOFC) as well as a variety of electrical applications, solid state electrolytes and high oxygen storage capability [9]. Also, the addition of CeO_2 causes to improve the proton conductivity which is appropriate for hydrogen separation membrane due to the induction of the electron conductivity by a rapid reduction of Ce^{4+} to Ce^{3+} at high temperature under the reduction condition [10]. In common with CeO_2, nickel oxide (NiO) has been researched for the applications such as catalyst, electrochromic device and fuel cell, because of its high catalytic activity and electrical properties [11]. In order to obtain the CeO_2-NiO mixed oxides which have the properties as above, the efficient sol-gel process is possible to produce

homogenous powder undergoing chemical method and has a lot of advantages [12]. Therefore, the purpose of this present study is the preparation of the CeO_2-NiO/SiC membranes and the effect of the CeO_2-NiO/SiC membrane on hydrogen permeation will be mainly discussed.

4.2 Experimental

4.2.1 Preparation of CeO_2-NiO mixed oxides

Cerium (III) nitrate hexahydrate ($Ce(NO_3)_3 \cdot 6H_2O$) and Nickel (II) nitrate hexahydrate ($Ni(NO_3)_2 \cdot 6H_2O$) with a purity of 99% (Aldrich) were dissolved into distilled water and stirred at 353 K for 1 h. As a catalyst, Nitric acid (HNO_3) (98%) was added so that the concentration of pH in the solution was adjusted. The sol solution was refluxed for 24 h and dried overnight at 393 K. The obtained gel powders were heat-treated to complete sol-gel reaction at 1173 K under air condition. Then, the CeO_2-NiO mixed oxides were successfully prepared.

4.2.2 Fabrication of CeO_2-NiO/SiC composites membrane

SiC (325 mesh, BIT Co., Ltd) was ball-milled (280 rpm) with the different χ wt% CeO_2-NiO contents (χ = 20, 40, 60 and 80) and 10 wt% Ni was used as a binder in order that the solid-state

reaction advances more effectively. The powder mixtures were pressed by uniaxial pressing at 15 MPa. All of the membranes were fabricated by hot-press sintering (HPS) through a mechanical alloying process at 1173 K under vacuum condition.

4.2.3 Characterization

The phase identification of the CeO_2-NiO/SiC mixture powders with increasing content of CeO_2-NiO mixed oxides were performed to determine the crystal structure by X-ray diffraction (XRD) (Bruker D8, Focus, Cukα, 40 Kv, 40 mA) instrument and the powders and hot-press sintered membranes were observed by field emission-scanning electron microscope (FE-SEM) (JEOL-JMS 7500F). Pore size distribution and porosity were analyzed by BJH (Barrett-Joyner-Halenda) and Archimedes method. The Brunner-Emmett-Teller (BET) was measured by the adsorption-desorption of N_2 gas per surface area (m^2/g) (BELSORP-max, mini II). For the hydrogen permeation test, the equipment consisted of a pressure controller, mass flow controller (MFC) and stainless

steel 1.4-inch cell module which was constructed as to withstand on high temperature. The membranes of different CeO_2-NiO contents were used for the evaluation of hydrogen permeation with a heating rate of 278 K/min under air condition up to 523 K under 0.1 MPa.

4.3 Results and Discussion

Fig. 1 (a) and (b) show the CeO_2-NiO mixed oxides and SiC powders before the hot-press sintering (HPS) process. As can been seen in Fig. 1 (a), the CeO_2-NiO mixed oxides have spherical shape and show such fine grains. The morphology of SiC powders observed by micro-scale is pointed at the end and a bigger size than the CeO_2-NiO mixed oxides is observed on the nano-scale in Fig. 1 (b) According to the growth of χ wt% CeO_2-NiO content (χ = 20, 40, 60 and 80), all the membranes between 20° and 80° ranges of XRD were investigated as shown in Fig. 2. The peaks of CeO_2-NiO mixed oxides shift higher and have sharp intensity, indicating crystallite growth. This suggests that the increasing content of mixing with CeO_2-NiO mixed oxides have sufficiently progressed. From the refinement of the crystal structure, the SiC peaks are the highest intensity among the phases including the hexagonal structure of α-SiC (JCPDS file No. 01-074-1302) with lattice constant of a = b = 0.308 Å and c = 15.11 Å. Also, CeO_2 of fluorite structure (JCPDS file No. 01-089-

8436) have cubic crystal system, whereas NiO (JCPDS file No. 00-044-1159) have a hexagonal (Rh) structure. These powder mixtures were later used for hot-press sintering (HPS). The results of hydrogen permeation flux are summarized in Fig. 3 (a). The hydrogen permeation has a similar trendy for all of the CeO_2-NiO/SiC membranes following the increasing temperature. When the temperature is increased from 323 K to 523 K at 0.1 MPa, the hydrogen permeation flux tends to be decreased except for the range of 303 K to 323 K and the hydrogen permeation flux increases below 323 K, where it reached a higher value than ever before. The ability of hydrogen permeation on the 80 wt% CeO_2-NiO/SiC membrane which has the highest flux made a distinction among all the membranes and the value at 323 K was obtained at 2.92×10^{-6} mol/m^2sPa. Otherwise, the 20 wt% CeO_2-NiO/SiC membrane of the hydrogen permeation flux at 303 K has the lowest value of 5.62×10^{-6} mol/m^2sPa. Fig. 3 (b) shows that χ wt% CeO_2-NiO/SiC membranes (χ = 20, 40, 60 and 80) have reacted as located by endothermic within the range of temperature 303 K to 323 in accordance with the Arrhenius plots. On the other hand, it

is shown the reaction of exothermic when the temperature was over 323 K. The flux of hydrogen permeation by the 80 wt% CeO_2-NiO/SiC membrane has considerably risen above the other membranes' maximum value. In Fig. 4, the 80 wt% CeO_2-NiO/SiC membrane which has the highest hydrogen permeation flux is indicated. Before the test, the surface showed that the CeO_2-NiO mixed oxides were blended with SiC powders and that the size of grains seems to be smaller than the membrane which is conducted by hydrogen permeation test from the surface. Fig. 5 (a) illustrates that all the CeO_2-NiO/SiC membranes are analyzed as type IV isotherm with a hysteresis loop defined by IUPAC (International Union of Pure and Applied Chemistry). Based on the results of BET surface area (m^2/g) by N_2 adsorption-desorption isotherms as shown in Fig. 5(a), all the CeO_2-NiO/SiC membranes are mesoporous as pore structure and the BET values increase with increasing contents of the CeO_2-NiO mixed oxides. In terms of pore size, these membranes have a pore size larger than 2 nm and smaller than 50 nm. The formation of mesopores

was referred to Knudsen diffusion mechanism which is in inverse proportion to the increasing temperature.

By means of Archimedes method, all the CeO_2-NiO/SiC membranes porosities were respectively measured and the porosity was approximately 31-32%. Regardless of porosity, the 80 wt% CeO_2-NiO/SiC membrane has shown the highest flux between 20 and 80 wt% membranes. The pore size distribution of the CeO_2-NiO/SiC membranes is presented in Fig. 5(b).

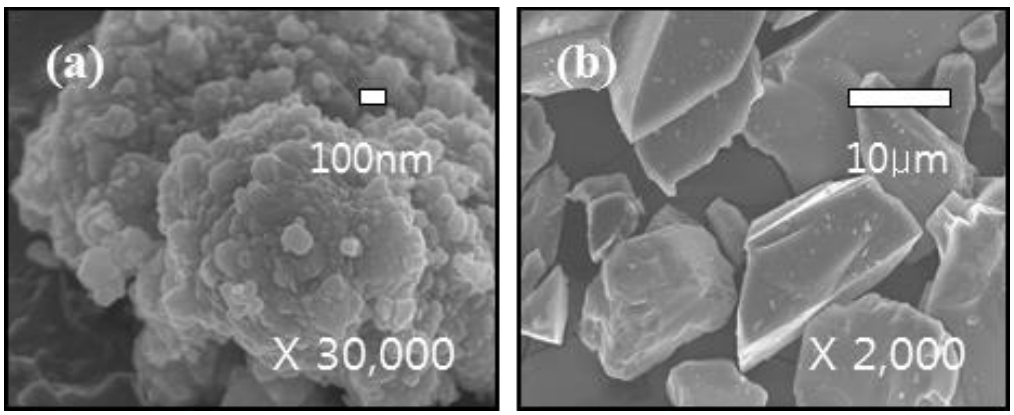

Fig. 1. FE-SEM images of (a) CeO_2-NiO mixed oxides sintered at 1173 K under air condition and (b) SiC powders

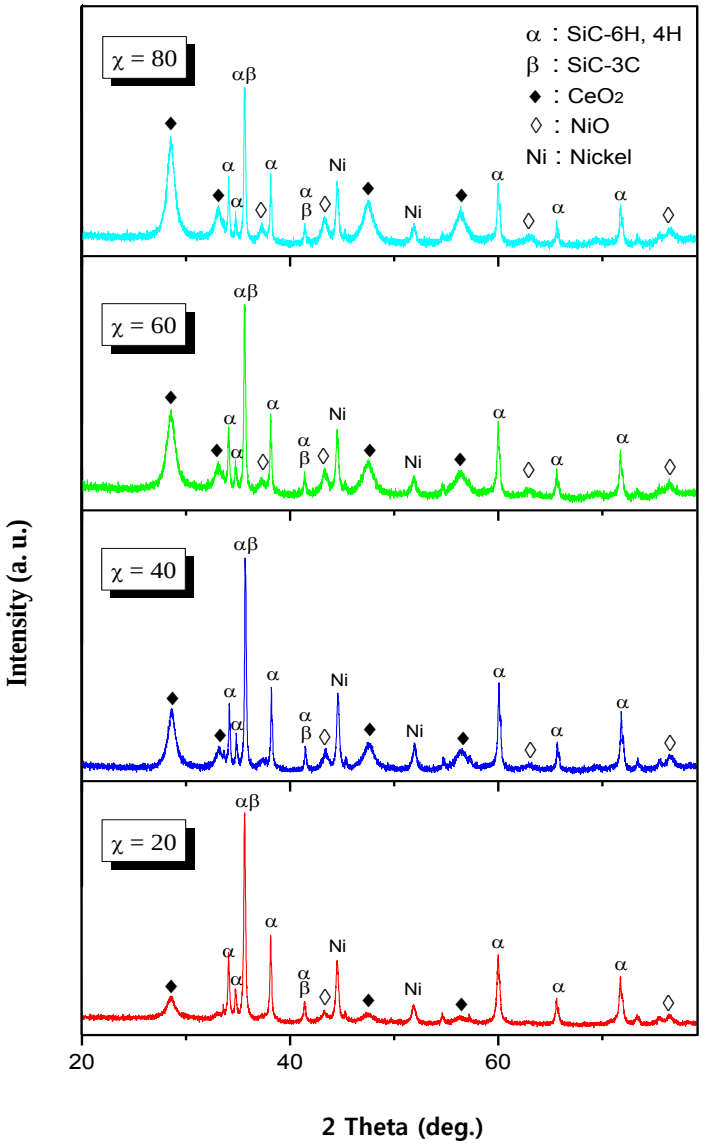

Fig. 2. XRD patterns of χ wt% CeO_2-NiO/SiC mixture powders (χ = 20, 40, 60 and 80).

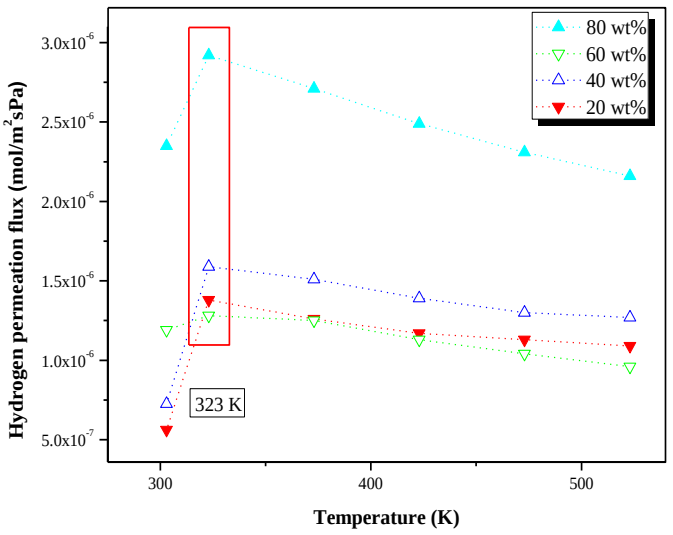

(a)

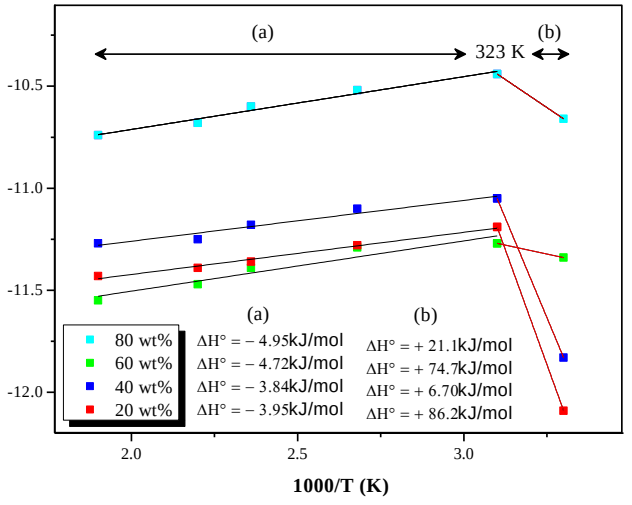

(b)

Fig. 3 (a) Hydrogen permeation fluxes of χ wt% CeO_2–NiO/SiC (χ = 20, 40, 60 and 80) and (b) Arrhenius plots on hydrogen permeation of all the CeO_2–NiO/SiC membranes.

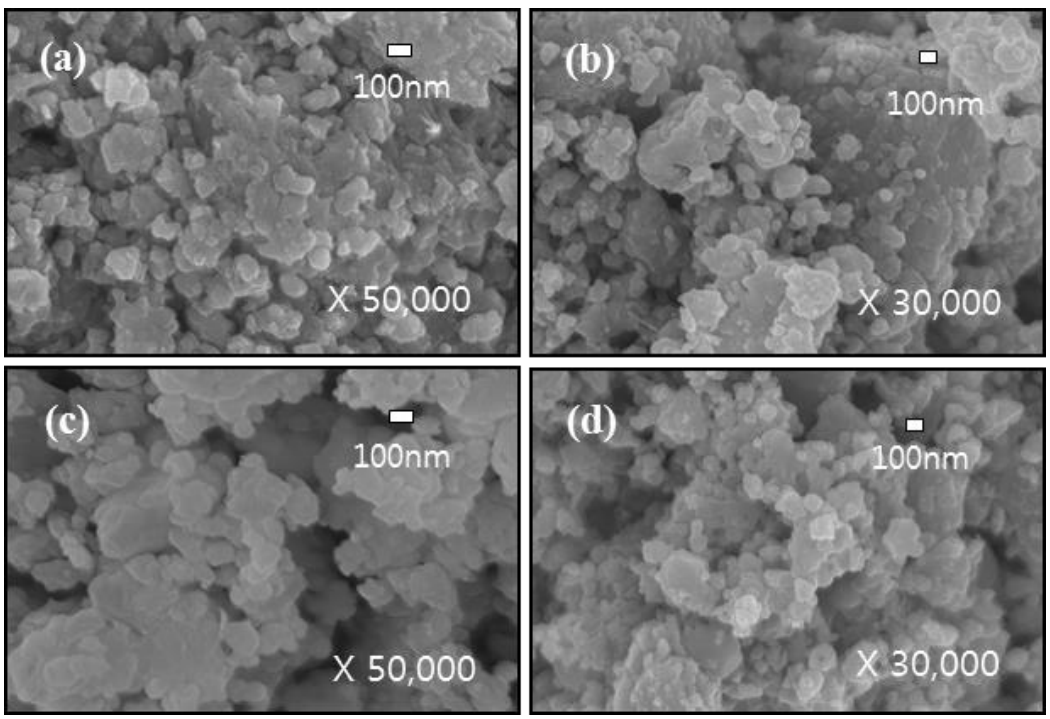

Fig. 4. FE-SEM images of (a) surface and (b) cross section before hydrogen permeation test and (c) surface and (d) cross section after hydrogen permeation test.

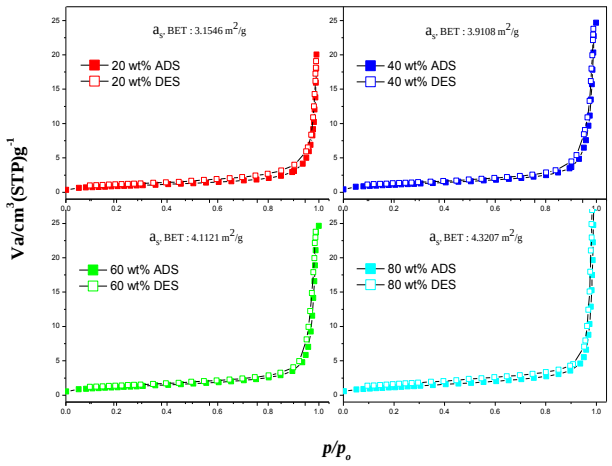

(a)

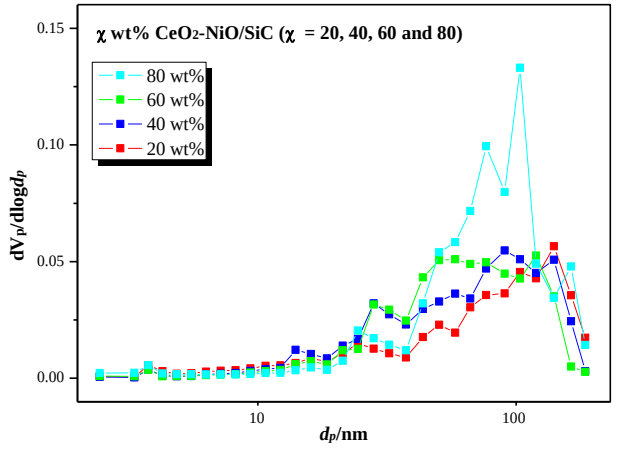

(b)

Fig. 5 (a) N_2 adsorption-desorption isotherms of all the CeO_2-NiO/SiC membranes and (b) Pore size distribution of CeO_2-NiO/SiC membranes.

4.4 Conclusion

The CeO_2-NiO membranes based on SiC have been successfully prepared for the evaluation of hydrogen permeation from 303 K to 523 K under 0.1 MPa. In increasing contents of CeO_2-NiO mixed oxides (20, 40, 60 and 80 wt%), the hydrogen permeation flux is followed a tendency to increase. Allowing it was uniform in size of porosity at 31-32 %, the 80 wt% CeO_2-NiO/SiC membrane has the highest hydrogen permeation flux as 2.92×10^{-6} mol/m^2sPa at 323 K. The activation energy (ΔH) of the membrane was calculated as -4.95 kJ/mol above 323 K and as +21.1 kJ/mol below 323 K, respectively

Reference

Chapter 1.

[1] H. A. Meinema, R. W. J. Dirrix, H. W. Brinkman, R. A. Terpstra, J. Jekerie and P. J. Kosters, Interceram., 54 86-91 (2005).

[2] B. Zapata, M. A. Valenzuela, J. Palacios and E. T. Garcia, Int. J. Hydrogen. Energ., 35 12091-12097 (2010).

[3] J.W. Phair, S.P.S. Badwal, Ionics 12 (2006) 103-115

[4] B. Zornoza, C. Casado and A. Navajas: Renewable Hydrogen Technologies, 245-266 (2013).

[5] F. Gallucci, E. Fernandez, P. Corengia and M. V. S. Annaland, Chem. Eng. Tehcnol., 92 40-66 (2013).

[6] J. Li, Y. Hao, H. Li, M. Xia, X. Sun and L. Wang, Micropor. Mesopor. Mat., 120 421-425 (2009).

[7] L. J. Duhamel, H. Zarrou and A. D. Huysser, Int. J. Hydrogen. Energ., 33 5527-5534 (2008).

[8] Y. Wang, C. Wang, C. Li, Y. Cheng and F. Chi, Ceram. Int., (In Press).

[9] Z. H. Song, W. Yuan, L. Gang, C. Xiao-ge and W. X. Li, J. Alloy. Compd, 537 141-146 (2012).

[10] Z. Hongsong, L. Ziaochun, L. Gang and L. Zhenjun, Ceram. Int., (In Press)

[11] V. Besikiotis, C. S. Knee, I. Ahmed, R. Haugsrud and T. Norby, Solid. State. Ionics., 228 1-7 (2012).

[12] W. Ma, S. K. Gong, H. B. Xu and X. Q. Cao, Surf. Coat. Tech., 200 5113-5118 (2006).

Chapter 2.

[1] S. H. Kim, Y. W. Kim, J. Y. Yun, and H. D. Kim, *J. Kor. Ceram. Soc.*, 41, 541 (2004).

[2] S. Liu, Y. P. Zeng, and D. Jiang, *J. Eur. Ceram. Soc.*, 29, 1795 (2009).

[3] Y. Zhou, K. Hirao, K. Watari, Y. Yamauchi, and S. Kanzaki, *J. Eur.Ceram. Soc.*, 24, 265 (2004).

[4] C. Vincent, J. F. Silvain, J. M. Heintz, and N. Chandra, *J. Phys. Chem.Solids.,*73, 499 (2012).

[5] M. Aparicio and A. Duran, *Ceram. Int.*, 31, 631 (2005).

[6] C. Sangwichien, G. L. Aranovich, and M. D. Donohue, *Colloid Surface,* 206, 313 (2002).

[7] R. Yamada, N. Igawa, and T. Taguchi, *J. Nucl. Mater.* 329, 497 (2004).

[8] M. Miu, M. Danila, I. Kleps, A. Braqaru, and M. Simion, *J. Nanosci.Nanotechnol.,* 11, 9136 (2011).

[9] A. Bakhsh and A. Maqsood, Electron. Mater. Lett. 8 605 (2012).

Chapter 3.

[1] B. Ernst, S. Haag and M. Burgard, J. Membrane. Sci., 288 208-217 (2007).

[2] F. Roa, J.D. Way, R.L. McCormick and S.N. Paglieri, Chem. Eng. J., 93 11-22 (2003).

[3] S. H. Kim, Y. W. Kim, J. Y. Yun and H. D. Kim, J. Kor. Ceram. Soc., 41 541-547 (2004).

[4] S. Liu, Y. P. Zeng and D. Jiang, J. Eur. Ceram. Soc., 29 1795-1802 (2009).

[5] Y. Zhou, K. Hirao, K. Watari, Y. Yamauchi and S. Kanzaki, J. Eur. Ceram. Soc., 24 265-270 (2009).

[6] J. H. Park, Y. H. Kim and M. W. Jung, J. Kor. Ceram. Soc., 49 412-416 (2012).

[7] C. Vincent, J. F. Silvain, J. M. Heintz and N. Chandra, J. Phys. Chem. Solids., 73 499-504 (2012).

[8] M. Aparicio, A. Duran, Ceram. Int., 31 631-634 (2005).

[9] A. K. Bhosale, P. S. Shinde, N. L. Tarwal, P. M. Kadam, S. S. Mali and P. S. Patil, Sol. Energ. Mat. Sol. C., 94 781-787 (2010).

Chapter 4.

[1] B. Ernst, S. Haag, M. Burgard, J. Membrane. Sci., Vol. 288, 208-217 (2007).

[2] F. Roa, J.D. Way, R.L. McCormick, S.N. Paglieri, Chem. Eng. J., Vol. 93, 11-22 (2003).

[3] J.W. Phair, S.P.S. Badwal, Ionics, Vol. 12, 103-115 (2006).

[4] A.E. Lewis, D.C. Kershner, S.N. Paglieri, M.J. Slepicka, J.D. Way, J. Membrane. Sci., Vol. 437, 257-264 (2013).

[5] K. Soongprasit, D.A. Ong, V. Sricharoenchaikul, D. Atong, Curr. Appl. Phys., Vol. 12, S80-S88 (2012).

[6] J. Park, Y. Kim, M. Jung, J. Ceram. Soc., Vol. 49, 412-416 (2012).

[7] R.A. Wash, M. Sugimoto, A. Idesaki, M. Yoshikawa, Mater. Sci. Eng., Vol. 140, 81-89 (2007).

[8] J.S. Lian, X.Y. Zhang, Z.H. Jiang, J. Zhang, Mater. Lett., Vol. 58, 1183-1188 (2004).

[9] J. Li, Y. Hao, H. Li, M. Xia, X. Sun, L. Wang, Micropor. Mesopor. Mat,. Vol. 120, 421-425 (2009).

[10] S. Huang, L. Li, O. Van der Biest, J. Vleugels, Solid State Ionics, Vol. 7, 539-544 (2005).

[11] W. Guo, K.N. Hui, K.S. Hui, Mater. Lett., 92, 291-295 (2013).

[12] M. Seyedahmadian, S. Houshyarazar, A. Amirshaghaghi, B. Kor. Chem. Soc., Vol. 34, 622-628 (2013).

[13] L.J. Duhamel, A. Ponchel, C. Lamonier, A. DHuysser, Y. Barbaux, Langmuir, Vol. 17, 1511-1517 (2001).

논문개요

수소분리막용 Ce계 세라믹스 멤브레인의 수소투과 특성평가

Jihye Park

Department of Chemistry

Graduate School of

Sungshin Women's University

졸-겔 (Sol-gel) 법은 저온에서 합성이 가능하고 그 과정 또한 용이하며 고순도 재료를 제조할 수 있다는 장점이 있다. 이 졸-겔 법을 사용하여 희토류계 금속인 세륨 (Ce)을 바탕으로 복합산화물을 합성하였다. 수소분리막은 디스크 형태의 멤브레인으로 성형하였으며, 수소투과실험을 위하여 높은 열전도도 및 열적 안정성과 내구성이 강한 실리콘 카바이드 (SiC) 슬러지 분말을 딥-코팅 과정을 통해 제조하였다. 태양광 및 반도체 산업의 실리콘 잉곳 절단과정에서 발생하는 실리콘카바이드를 실험에 재활용하여 사용하는 것은 산업폐기물의 양을 줄임과 동시에 친환 경적인 그린케미스트리가 될 수 있다. 또한 기계적 강도가 크고 높은 연성을 가지는 니켈(Ni) 금속 분말을 세륨과 기계적 합금화법으로 혼합하고, 열간 압축 성형법을 이용하여 써멧 (Cermet) (세라믹스/금속) 분리막을 제조하였다.

써멧 분리막의 경우 합성 분말의 함량이 증가함에 따라 투과도는 향상되지만 선택성이 감소하는 단점이 있었다. 따라서 수소분위기에서 환원이 빠르게 진행되는 세륨의 문제점을 보완함과 동시에 선택도를 높이기 위하여 $A_2B_2O_7$ 의 형석 (Fluorite) 구조를 갖는 란탄세라이트를 합성하였다. 합성한 분말을 이용하여 제조한 수소분리용 멤브레인은 XRD, TOPAZ, FE-SEM, EDS, BET 를 사용하여 특성 평가를 진행하였고, 수소 투과 특성평가는 다양한 압력과 온도 하에서 수소 가스를 투과하여 진행하였다.